Spectrum of $K_V2.1$ Dysfunction in *KCNB1*-Associated Neurodevelopmental Disorders

Seok Kyu Kang, MS,[1]* Carlos G. Vanoye, PhD,[1]* Sunita N. Misra, MD, PhD,[1,2,3] Dennis M. Echevarria, BA,[1] Jeffrey D. Calhoun, PhD,[1] John B. O'Connor, MS,[3] Katarina L. Fabre, MS,[1] Dianalee McKnight, PhD,[4] Laurie Demmer, MD,[5] Paula Goldenberg, MD,[6] Lauren E. Grote, MS, CGC,[7,8] Isabelle Thiffault, PhD,[8,9,10] Carol Saunders, PhD,[8,9,10] Kevin A. Strauss, MD,[11] Ali Torkamani, PhD,[12] Jasper van der Smagt, MD, PhD,[13] Koen van Gassen, PhD,[13] Robert P. Carson, MD, PhD,[14] Jullianne Diaz, MS, CGC,[15] Eyby Leon, MD,[15] Joseph E. Jacher, MS, CGC,[16] Mark C. Hannibal, MD,[16] Jessica Litwin, MD,[17] Neil R. Friedman, MBChB,[18] Allison Schreiber, MS, LGC,[18] Bryan Lynch, MB,[19] Annapurna Poduri, MD, MPH,[20] Eric D. Marsh, MD, PhD,[21] Ethan M. Goldberg, MD, PhD,[21] John J. Millichap, MD,[2,3,22] Alfred L. George Jr MD,[1] and Jennifer A. Kearney, PhD[1]

Objective: Pathogenic variants in *KCNB1*, encoding the voltage-gated potassium channel $K_V2.1$, are associated with developmental and epileptic encephalopathy (DEE). Previous functional studies on a limited number of *KCNB1* variants indicated a range of molecular mechanisms by which variants affect channel function, including loss of voltage sensitivity, loss of ion selectivity, and reduced cell-surface expression.
Methods: We evaluated a series of 17 *KCNB1* variants associated with DEE or other neurodevelopmental disorders (NDDs) to rapidly ascertain channel dysfunction using high-throughput functional assays. Specifically, we investigated the biophysical properties and cell-surface expression of variant $K_V2.1$ channels expressed in heterologous cells using high-throughput automated electrophysiology and immunocytochemistry–flow cytometry.
Results: Pathogenic variants exhibited diverse functional defects, including altered current density and shifts in the voltage dependence of activation and/or inactivation, as homotetramers or when coexpressed with wild-type $K_V2.1$.

View this article online at wileyonlinelibrary.com. DOI: 10.1002/ana.25607

Received Jun 13, 2019, and in revised form Sep 16, 2019. Accepted for publication Sep 16, 2019.

Address correspondence to Dr Kearney, 320 East Superior St, Searle 8-510, Chicago, IL 60611. E-mail: jennifer.kearney@northwestern.edu

*S.K.K. and C.G.V. contributed equally.

From the Departments of [1]Pharmacology and [2]Pediatrics, Northwestern University Feinberg School of Medicine, Chicago, IL; [3]Ann & Robert H. Lurie Children's Hospital of Chicago, Chicago, IL; [4]GeneDX, Gaithersburg, MD; [5]Department of Pediatrics, Atrium Health's Levine Children's Hospital, Charlotte, NC; [6]Medical Genetics, Massachusetts General Hospital for Children, Harvard Medical School, Boston, MA; [7]Division of Clinical Genetics, Children's Mercy Hospital, Kansas City, MO; [8]University of Missouri–Kansas City School of Medicine, Kansas City, MO; [9]Center for Pediatric Genomic Medicine and [10]Department of Pathology and Laboratory Medicine, Children's Mercy Hospital, Kansas City, MO; [11]Clinic for Special Children, Strasburg, PA; [12]Scripps Translational Science Institute and Scripps Research Institute, La Jolla, CA; [13]Department of Genetics, University Medical Center Utrecht, Utrecht, the Netherlands; [14]Monroe Carell Jr Children's Hospital at Vanderbilt, Nashville, TN; [15]Rare Disease Institute, Children's National Medical Center, Washington, DC; [16]Division of Pediatric Genetics, Metabolism, and Genomic Medicine, University of Michigan, Ann Arbor, MI; [17]University of California, San Francisco Benioff Children's Hospital, San Francisco, CA; [18]Cleveland Clinic Children's, Cleveland, OH; [19]Department of Paediatric Neurology and Clinical Neurophysiology, Children's University Hospital, Dublin, Ireland; [20]Epilepsy Genetics Program, Department of Neurology, Boston Children's Hospital, Harvard Medical School, Boston, MA; [21]Division of Child Neurology, Children's Hospital of Philadelphia, Philadelphia, PA; and [22]Department of Neurology, Northwestern University Feinberg School of Medicine, Chicago, IL

Additional supporting information can be found in the online version of this article.

Quantification of protein expression also identified variants with reduced total $K_V2.1$ expression or deficient cell-surface expression.

Interpretation: Our study establishes a platform for rapid screening of $K_V2.1$ functional defects caused by *KCNB1* variants associated with DEE and other NDDs. This will aid in establishing *KCNB1* variant pathogenicity and the mechanism of dysfunction, which will enable targeted strategies for therapeutic intervention based on molecular phenotype.

ANN NEUROL 2019;86:899–912

De novo variants in a diverse range of genes constitute a significant cause of developmental and epileptic encephalopathy (DEE) and other neurodevelopmental disorders (NDDs).[1,2] Despite an increasing number of genes identified for DEE and increased clinical genetic testing, many variants are classified as variants of uncertain significance that are difficult to interpret and/or act on. Obtaining functional data is a powerful approach to bridge the knowledge gap between genetics and molecular pathology,[3] which can provide additional evidence for interpretation of variant pathogenicity and offer functional information to guide treatment strategies. However, due to the low throughput of many functional assays, functional annotation of variants is a major bottleneck in the field. The development of high-throughput assays is a necessary step for experimental evaluation of the large volume of novel variants being identified by increased clinical genetic testing.

KCNB1 (NM004975) encodes the $K_V2.1$ voltage-gated potassium (K^+) channel α-subunit that conducts delayed rectifier K^+ current,[4] a key modulator of membrane repolarization in electrically excitable cells, including various neuron subtypes.[5] *Kcnb1*-deficient mice display enhanced seizure susceptibility and behavioral hyperexcitability, indicating that $K_V2.1$ acts as a homeostatic suppressor of heightened neuronal activity.[6] De novo missense variants in *KCNB1* are associated with DEE,[7–13] which includes multiple seizure types, developmental delay, and neuropsychiatric sequelae. Correlational analyses based solely on the substituted amino acid type and position have proven insufficient for genotype–phenotype association,[11] highlighting the need for experimental studies to determine functional effects of additional variants. To date, 7 *KCNB1* variants associated with DEE, all located in the pore (S347R, T374I, V378A, G379R, G401R) and voltage-sensor (I199F, R306C) domains, have been shown to exhibit altered potassium current density, voltage dependence, and/or ion selectivity.[7–9,14] However, determining the functional consequences of a larger series of variants is necessary to define the range of dysfunction and broaden the associated clinical phenotypes studied.

In this study, we performed high-throughput functional studies of 19 *KCNB1* variants (17 missense, 1 frameshift, 1 nonsense) to determine their effect on protein function and provide functional evidence for weighing potential pathogenicity. Several broad categories of channel dysfunction (ie, altered peak current density, voltage dependence, protein expression) were identified, and most variants conferred some degree of loss of function. Our results provide insight into functional pathogenicity for a large series of *KCNB1* variants. This will aid in prioritization for development of more complex experimental models (ie, knockin mouse or induced pluripotent stem cells) by identifying a subset of representative variants based on underlying pathophysiologic mechanisms. Uncovering a range of *KCNB1* functional defects will help define genotype–phenotype relationships by adding a molecular phenotype to the genotypes, and may ultimately enable development of targeted treatment strategies for individuals with *KCNB1* DEE.

Materials and Methods

Information was collected for individuals with DEE or other NDDs and a potentially pathogenic *KCNB1* variant (identified as part of routine care) under approval of the Ann & Robert H. Lurie Children's Hospital of Chicago Institutional Review Board (IRB) or through collection of deidentified information deemed non–human subjects research by the Northwestern University IRB. Consent for release of deidentified information was obtained in accordance with local institutional policies. In addition, 11 *KCNB1* variants were obtained from the literature and variant databases.[8–13,15–19] No functional studies were available for 17 of 19 variants.

Plasmids

Full-length human *KCNB1* cDNA in plasmid pIRES2-DsRed-MST-$K_V2.1$-WT (Addgene, Cambridge, MA; #131707) was described.[7,14] For cotransfections, pIRES2-smGFP-KV2.1-WT (Addgene #131709) was engineered by replacing DsRed-MST with smGFP, allowing detection of WT + variant cells (Addgene #131709). For cell-surface labeling, a 2xHA-tag was inserted between amino acids 220 and 221, and the IRES2-DsRed-MST cassette was removed, resulting in pCMV-$K_V2.1$-HA-WT. Variants were introduced using QuikChange mutagenesis (Agilent Technologies, Santa Clara, CA). Clones were sequenced to confirm desired modifications and absence of unwanted mutations.

Heterologous Expression

Transient expression of wild-type (WT) and variant $K_V2.1$ in CHO-K1 cells (CRL 9618; ATCC, Manassas, VA) was achieved by electroporation using the STX system (MaxCyte, Gaithersburg, MD) with the preset CHO or CHO-PE protocol (7.5–10μg KCNB1 cDNA per $1e^7$ cells). Following electroporation, cells were grown for 36 hours, harvested, and frozen in liquid N_2. Coexpression of WT and variant was achieved by coelectroporation of pIRES2-DsRed-MST-$K_V2.1$-WT or -variant (5μg) plus pIRES2-smGFP-$K_V2.1$-WT (5μg).

Cell Preparation for Automated Patch Clamp Recording

Cells were thawed, incubated for 24 hours, and harvested using 0.25% trypsin–ethylenediaminetetraacetic acid in F-12K media (GIBCO/Invitrogen, Waltham, MA) supplemented with 10% fetal bovine serum (Atlanta Biologicals, Flowery Branch, GA). Cell number and viability were determined (Vi-Cell; Beckman Coulter, Fullerton, CA). Cells were diluted to 200,000cells/ml with external solution (see below) and allowed to recover for 40 minutes at 15°C, shaking at 200rpm.

Automated Patch Clamp Recording

Automated patch clamp recording was performed using the SyncroPatch 768PE system (Nanion Technologies, Munich, Germany). External solution contained (in mM): 140 NaCl, 4 KCl, 1 $MgCl_2$, 2 $CaCl_2$, 5 glucose, and 10 hydroxyethylpiperazine ethane sulfonic acid (HEPES), pH 7.4. Internal solution contained (in mM): 60 KF, 50 KCl, 10 NaCl, 20 ethyleneglycoltetraacetic acid, 10 HEPES, pH 7.2. Pulse generation and data collection used PatchController 384 V1.3.0 and DataController384 V1.2.1 software (Nanion Technologies). Whole-cell currents were acquired at 5kHz and filtered at 1kHz. Currents were not leak subtracted. Access resistance and apparent membrane capacitance were estimated using built-in protocols. Whole-cell currents were measured at room temperature from a holding potential of −80mV and elicited with depolarizing steps (500 milliseconds) from −100 to +60mV (10mV steps) followed by a 250-millisecond step to −30mV or 0mV (tail currents). Background currents were removed by digital subtraction of whole-cell currents recorded from nontransfected CHO-K1 cells offline. Current amplitudes were analyzed from all cells with seal resistance ≥0.5GΩ, series resistance ≤20MΩ, and cell capacitance >2pF. Electrically unstable cells with loss of seal or voltage control were excluded. The peak current (I_{peak}) was normalized for cell capacitance and plotted against voltage to generate current density–voltage relationships. Voltage dependence of activation was determined by plotting tail currents normalized to the largest tail current amplitude against the depolarizing test potential (−100 to +60 mV). Normalized G-V curves were fit with the Boltzmann function $G = 1 / (1 + \exp[(V - V_{½}) / k])$ to determine voltage for half-maximal channel activation ($V_{½}$) and slope factor (k). Voltage dependence of inactivation was assessed following a 5-second prepulse from −100 to +40mV (10mV steps) followed by a 250-millisecond step to +60mV. Normalized currents measured at the +60mV test potential were plotted against the prepulse voltage and fit with the Boltzmann function $(I/I_{max} = 1 / (1 + \exp[(V - V_{½}) / k])$ to determine $V_{½}$ and k. Voltage dependence of channel activation or inactivation was determined only from cells with positive outward current values following background subtraction. Statistical outliers (≥ ± 3 standard deviations) were excluded.

Immunocytochemistry–Flow Cytometry

Cells were electroporated as described above and incubated for 24 hours prior to labeling. For analysis of total and cell-surface expression, cells were incubated with αHA-Alexa488 (16B12; Thermo Fisher Scientific, Waltham, MA; 1:250 in fluorescence-activated cell sorting buffer [1% fetal bovine serum, 0.05% NaN_3 in phosphate-buffered saline, pH 7.4]). Cells were then harvested and fixed/permeabilized using Fix&Perm buffer (BD Biosciences, Franklin Lakes, NJ). Following permeabilization, $K_V2.1$ was detected using Alexa 647–conjugated anti-$K_V2.1$ mouse monoclonal antibody (K89/34, Antibodies Incorporated, Davis, CA; A20186, Thermo Fisher Scientific; 1:200 in Perm buffer with 3% normal goat serum). Fluorescence signals were measured by flow cytometry (CytoFlex, Beckman Coulter) and analyzed with CytExpert (Beckman Coulter) and FlowJo software (FlowJo, Ashland, OR). Nontransfected CHO-K1 cells processed identically served as negative controls. Light-scatter based gates (forward scatter/side scatter (FSC/SSC)) were used to exclude nonviable cells and cell debris. A total of 10,000 events were analyzed for each variant per experiment.

For independent analyses of $K_V2.1$ total expression, frozen aliquots of electroporated cells were thawed, cultured for 24 hours, and then directly harvested with Accutase, without cell-surface labeling. Percent positive variant-expressing cells were normalized to WT-expressing cells tested on the same day. Histograms were aligned to correct for between-run variability in fluorescence intensity; y-axes were uniformly set across conditions.

Cell-Surface Biotinylation and Immunoblotting

Frozen aliquots of CHO-K1 cells electroporated with WT or variant $K_V2.1$ channels were thawed and grown under the same conditions used for automated patch clamp recording. Cell-surface biotinylation and immunoblotting were performed as previously described,[7,14] 60 to 72 hours postelectroporation, using mouse anti-$K_V2.1$ (1:250; K89/34, Antibodies Incorporated), mouse anti–transferrin receptor (1:500; H68.4, Thermo Fisher Scientific), rabbit anticalnexin (1:250; H70; Santa Cruz Biotechnology, Santa Cruz, CA), Alexa Fluor 680–goat antirabbit IgG (1:20,000; Jackson ImmunoResearch, West Grove, PA), and Alexa Fluor 790–goat antimouse IgG (1:20,000, Jackson ImmunoResearch) antibodies.

Normalized total, surface, and surface/total protein ratio results were derived from 3 independent experiments. Calnexin immunoreactivity was present in total protein lysates and absent from the cell-surface fraction, confirming the selectivity of biotin labeling for cell-surface protein.

Data Analysis

Data were analyzed using DataController384 V1.2.1 (Nanion Technologies), SigmaPlot 2000 (Systat Software, San Jose, CA), Prism (GraphPad Software, San Diego, CA), and OriginPro 2018 (OriginLab, Northampton, MA). Variants were compared to WT using 1-way analysis of variance (ANOVA) with Dunnett post hoc comparisons or unpaired t tests. Normalizations and statistical comparisons to WT were conducted per plate (for electrophysiology) or per experiment (for protein expression) to account for potential batch effects. For voltage dependence in coexpression experiments, obtained parameters ($V_{1/2}$ or k) could not be subject to percentile normalization (multiple batches); thus, average values of WT and each variant were compared using Brown–Forsythe and Welch ANOVA with Dunnett T3 multiple comparisons. Data fits with Boltzmann's equation were done for each individual cell using nonlinear curve fitting in OriginPro 2018; solid fit lines represent fits of averaged data. Whole-cell currents normalized for membrane capacitance are expressed as mean ± standard error of the mean.

Principal component analysis (PCA) was performed using ClustVis,[20] with principal components (PCs) calculated using the Nipals algorithm. Six variables (homomeric) were compared: I_{peak} density, $V_{1/2}$ and k for activation and inactivation, and cell-surface/total expression ratio; all were normalized with respect to WT by percentile value or z score. Spearman nonparametric correlational analysis was performed using the leading variables from PCA with number of seizure types and age at onset.

Results

KCNB1 *Variant In Silico Analysis and Clinical Phenotypes*

KCNB1 variant residues reported here all show a high degree of evolutionary conservation (Fig 1A) and are located mainly in the transmembrane domains of $K_V2.1$ (see Fig 1B, C). S202, T210, R306, and R312 are located in the voltage-sensing domain.[21] R325 and E330 are in the S4–S5 linker, critical for electromechanical coupling between the voltage-sensing and pore domains.[22] W370, P385, K391, and F416 are in the pore domain, with V378 and G381 located within the selectivity filter.[23] Truncation variants at Y274 and Y533 are not predicted to undergo nonsense-mediated mRNA decay, as the premature stop codons are located in the last exon, and are likely to generate truncated proteins. All disease-associated (pathogenic/likely pathogenic) variants had a scaled Combined Annotation Dependent Depletion score of >22, indicating they rank among the top 1% of deleterious variants with respect to all possible single nucleotide variants in the reference genome (Supplementary Table 1).[24]

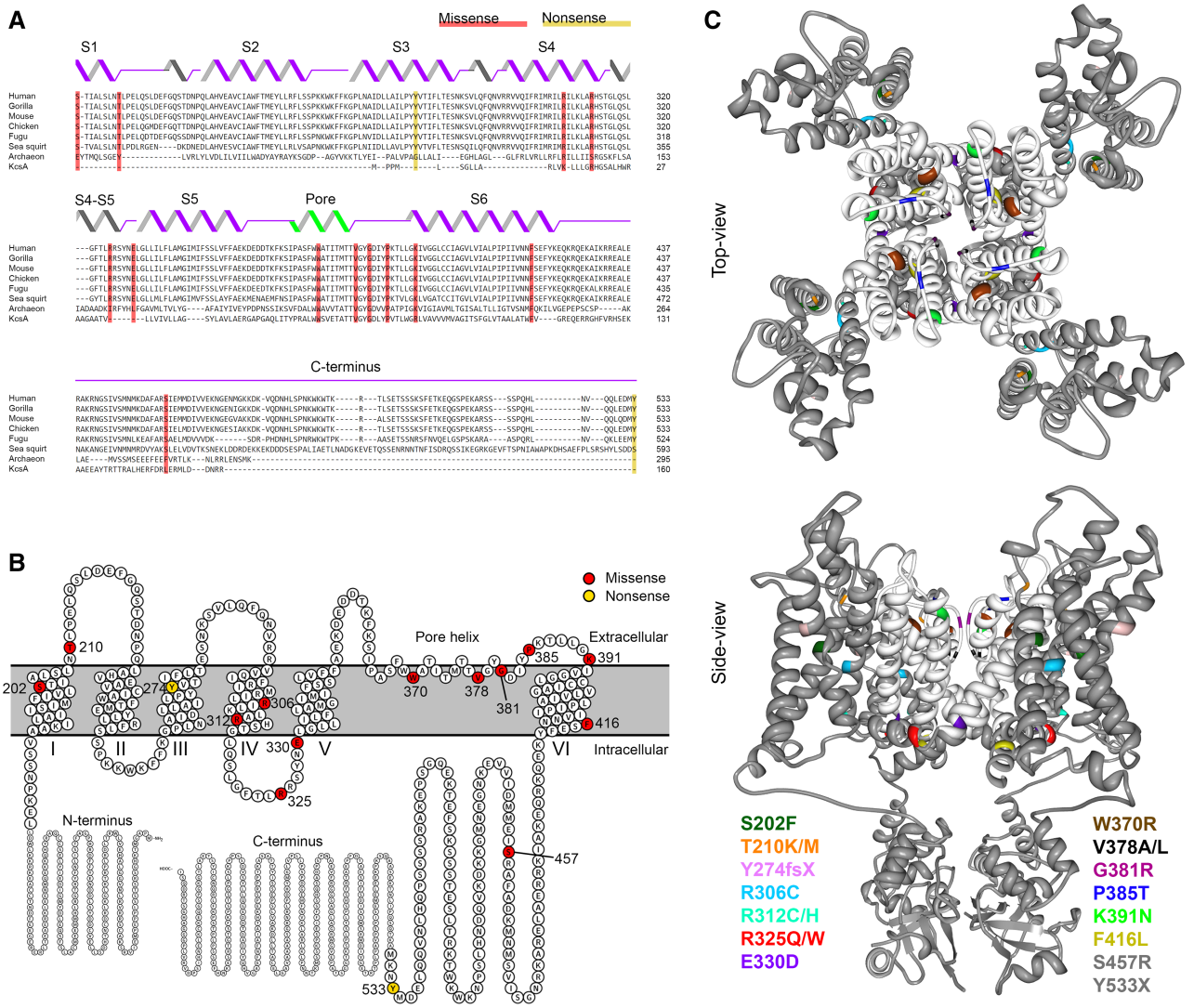

FIGURE 1: ***KCNB1*** **variants identified in individuals with developmental and epileptic encephalopathy. (A) Evolutionary conservation of $K_V2.1$ shown by multiple sequence alignment of $K_V2.1$ species orthologues (Clustal Omega[39]); secondary structural elements are illustrated above the sequences. $K_V2.1$ variants are shaded in red (missense) and yellow (nonsense). (B) Schematic view of the entire $K_V2.1$ subunit and the variants in the membrane, modified from Protter plot of Q14721 (KCNB1_Human).[40] (C) Locations of variants (color-coded) mapped onto crystal structure of $K_V2.1$/Kv1.2 chimera (PDB2R9R),[21] featuring a top view and a side view across a lipid bilayer. Pore domain is highlighted in white; 2 variants (S457R and Y533X) are not depicted, because their location in the distal C-terminus is not available in crystal structure. KcsA = K channel of streptomyces A.**

Clinical phenotypes summarized in Supplementary Table 1 include DEE in 28 patients and other NDDs in 4 patients. Among those with NDDs, 1 had a single seizure and 3 had no history of seizure at last reported follow-up at ≤6 years of age. Phenotypes for novel variants reported in Supplementary Table 1 are consistent with previous reports.[7–14] Supplementary Table 1 also includes variants from previous clinically focused reports,[11,16] summarized here for completeness, with updates when available. In total, there are 17 pathogenic/likely pathogenic variants from 27 individuals, including several recurrent variants (T210M × 3, R306C × 6, R312C × 2, R312H × 2, E330D × 2, V378A × 2, P385T × 2, F416L × 3).

Consequences of K_V2.1 Variants on Current Density

To screen for functional consequences of the *KCNB1* variants, we recorded whole-cell currents in voltage clamp mode of CHO-K1 cells transiently expressing WT or variant K_V2.1 channels using the SyncroPatch 768PE automated patch clamp platform (see Fig 2A). Previous studies showed feasibility of this approach to study channel properties of K_V2.1 and the closely related K_V7.1 channel encoded by *KCNQ1*.[14,25,26] In addition, we also tested on this platform the T374I variant that we previously characterized by manual patch clamp recording,[7] and reproduced the loss-of-function phenotype (see Fig 2B; $p < 0.001$, unpaired t test @ +60mV vs WT). This further validates use of this platform to screen for K_V2.1 dysfunction.

K_V2.1 channels are a tetrameric assembly of 4 alpha subunits encoded by *KCNB1*. When singly expressed in CHO cells, the K_V2.1 channels form a homomeric configuration of 4 WT or 4 variant subunits. In the homomeric configuration, the majority of the K_V2.1 variants (13/19) exhibited low K^+ conductance (loss of function; see Fig 2C, red), whereas the remaining variants displayed moderate K^+ conductance (partial loss of function; blue) or K^+ conductance similar to WT (gray). The degree of loss of function was considered "partial" if I_{peak} density was reduced 50 to 70% relative to WT and "severe" if >75%. Averaged whole-cell current density traces for K_V2.1 WT and representative variants are displayed to show diversity in current density (see Fig 2C, right). Averaged whole-cell I_{peak} density traces for all K_V2.1 variants are shown in Figure 3.

KCNB1 DEE is associated with de novo heterozygous variants. Thus, an individual has K_V2.1 subunits produced from both WT and variant alleles. To determine the effect of the *KCNB1* variants in a condition resembling heterozygosity in the patient, we coelectroporated each variant with WT channels at a 1:1 equimolar ratio. In the coexpression configuration (WT + variant), many variants exhibited I_{peak} density similar to cells transfected with WT + WT channels, suggesting that these variants can be rescued by WT coexpression. In contrast, W370R, P385T, and F416L exhibited significantly lower I_{peak} density compared to WT + WT cells (see Fig 2D, bars in red). These variants also showed lower I_{peak} density when compared to cells transfected with half the amount of WT plasmid (0.5× WT), suggesting a dominant-negative interaction of the variant with WT subunits. R306C and V378L exhibited partial loss of function (bars in turquoise) similar to 0.5× WT. Averaged current traces for a subset of variants are displayed (see Fig 2D, right). Complete statistical information including number of cells and p values are shown in Supplementary Table 2, and normalized traces are shown in Figure 3.

Total Protein Expression of K_V2.1 Variants

To test whether loss-of-function phenotypes with impaired current density were due to less channel protein, we evaluated total expression levels for K_V2.1 variants by immunoblotting and/or immunocytochemistry–flow cytometry (ICC-FC) using frozen aliquots of the same cells tested by electrophysiology. In the homomeric configuration, population analyses of K_V2.1-positive cells confirmed that *KCNB1* variants with severe loss-of-function phenotypes had less K_V2.1 protein compared to WT (see Fig 2E, G). The same variants coexpressed 1:1 with WT showed similar results. However, correlational analyses of current density and total protein expression showed no relationship between parameters in either homomeric ($R^2 = 0.16$, $p = 0.22$, Pearson correlation) or coexpression conditions ($R^2 = 0.0003$, $p = 0.96$; see Fig 2F, H). Variants not shown in Figure 2E and G were tested by immunoblotting (Fig 4E–G).

Expression Analysis of K_V2.1 Variants: Cell-Surface Trafficking

Presence at the cell-surface is critical for voltage-gated ion channel function, and some variants may interfere with K_V2.1 cell-surface expression. Cell-surface and total expression were simultaneously examined using ICC-FC. An extracellular hemagglutinin (HA)-epitope tag enabled discrimination of cell-surface and total K_V2.1 fractions, allowing rapid determination of cell-surface expression. A substantial population of WT K_V2.1 reached the cell-surface, with a mean surface/total expression ratio > 0.8 (see Fig 4A, B), indicating highly efficient cell-surface trafficking as previously shown.[29,30] The majority of the variants (13/19) exhibited deficits in cell-surface expression of K_V2.1, potentially explaining the loss of K^+ conductance observed by electrophysiology (see Fig 2C). The nonpathogenic variants (R325Q, S457R) exhibited cell-surface and total expression indistinguishable from WT (see Fig 4). Cross-validation of select variants (T210K/M, R312C, R325Q/W, V378A, K391N) with cell-surface biotinylation

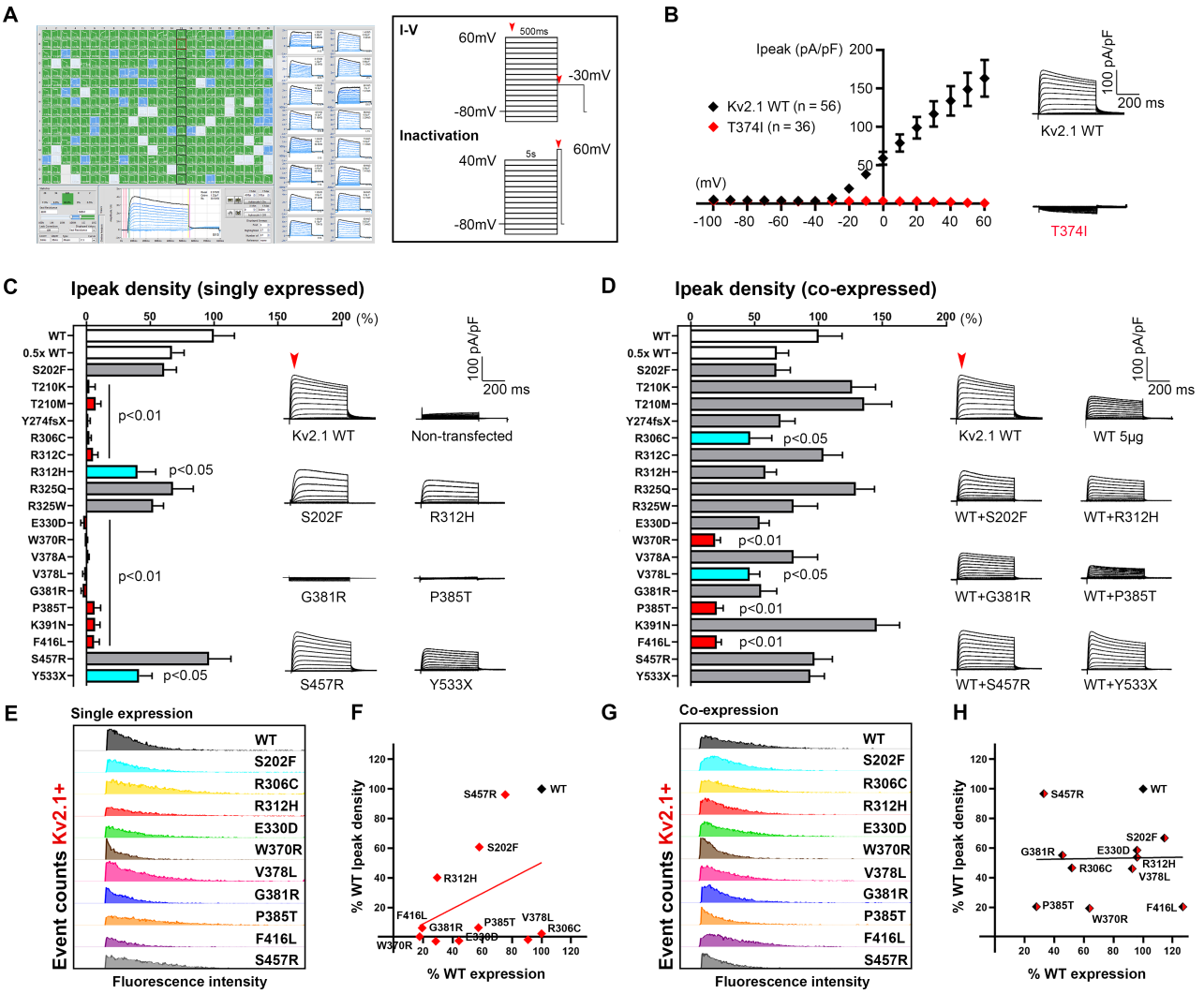

FIGURE 2: High-throughput functional screening of $K_V2.1$ variants. (A) Screenshot of automated whole-cell current recordings from CHO-K1 cells transiently expressing $K_V2.1$ channels, with 16 individual cell recordings shown on the right blue traces. Voltage protocols used for functional studies are depicted in the box; red arrowheads indicate time-points of current measurement. I-V = current–voltage. (B) Validation of automated patch clamp recordings of $K_V2.1$ channels. Averaged $K_V2.1$ wild-type (WT) and T374I variant (previously published by our group using manual patch clamp) current–voltage relationships and whole-cell current density traces show a similar loss-of-function phenotype for the T374I variant. (C, D) Comparison of peak current (I_{peak}) density of $K_V2.1$ variants in homomeric and coexpression (with WT) configuration (*red bars:* $p < 0.001$ vs WT, $p < 0.05$ vs 0.5 × WT; *turquoise bars:* $p < 0.05$ vs WT; 1-way analysis of variance Dunnett multiple comparisons). Averaged whole-cell current traces of selected variants are shown on the right; endogenous current recorded from nontransfected CHO-K1 cells were subtracted offline. Red arrowheads denote the time of I_{peak} measurement. For coexpression configuration, $K_V2.1$ variants were coexpressed with WT by electroporation of equimolar amount of DNA. (E, G) Protein expression analyses of variants by flow cytometry in the homomeric (left) and coexpression (right) configuration confirm $K_V2.1$ protein expression in variant-expressing cells, in particular for the ones with severely reduced current density, albeit with differing degrees of severity. Data are shown in histograms aligned to correct for between-run variability in fluorescence intensity; y-axes were uniformly set at a maximum of 250 and 350 event counts (for G and E, respectively) across conditions. (F, H) Correlation of I_{peak} density and protein expression by percentage $K_V2.1$-positive cells, in either homomeric or coexpression configuration, did not reach statistical significance ($p = 0.22$ and 0.96, respectively; Pearson correlation).

followed by immunoblotting produced largely congruent results. The observed reduction in protein expression for some variants that was not observed by ICC-FC is likely due to the time difference at which the proteins were analyzed. It is possible that during the extended time (an extra 24–36 hours compared to the ICC-FC experiment), variants may have triggered misfolded protein responses, which may slow down protein translation or induce cell death.

S202F, located near the HA-epitope site (amino acid 220), likely had altered immunoreactivity, considering the lack of anti-HA signal but intact current density of S202F. The substituted phenylalanine may result in steric hindrance, preventing HA antigen–antibody interaction. For the T210K/M variants, also located nearby the HA-tag site, immunoblotting of nontagged T210K/M confirmed lower cell-surface expression (see Fig 4A, B, E–G), consistent

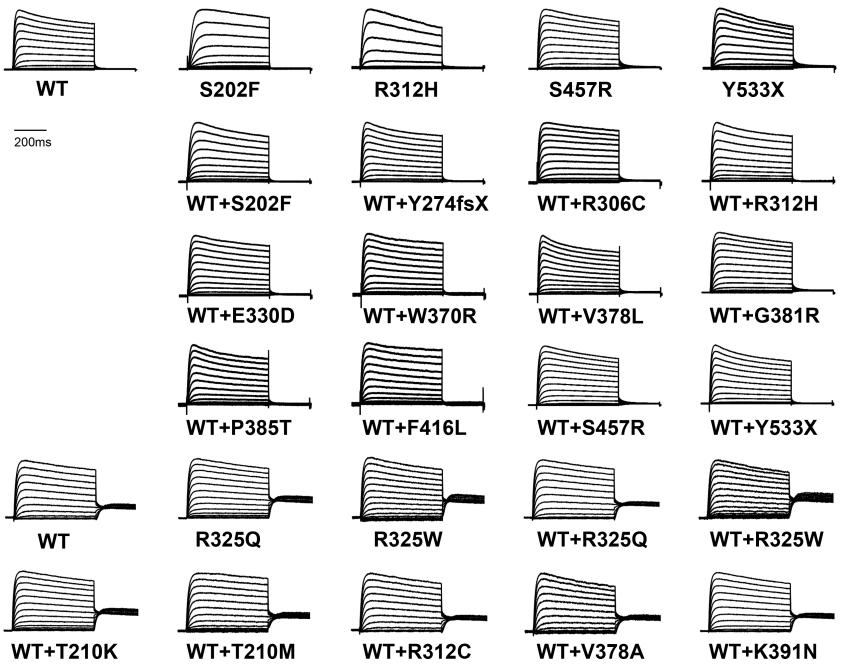

FIGURE 3: Averaged current density traces normalized to the maximal peak, showing averaged whole-cell currents recorded from CHO-K1 cells transiently expressing homomeric wild-type (WT) or variant K_V2.1, or coexpressing WT + variant K_V2.1 and normalized to the maximum peak current at +60mV. Traces were normalized to peak current to enable comparison of gating behaviors among variants with divergent current density. Horizontal scale bar represents 200 milliseconds.

with loss-of-function phenotypes in homomeric configuration (see Fig 2C).

The 2 truncation variants, Y274fsX36 and Y533X, were also tested for expression, despite lacking the epitope site for anti-Kv2.1–Alexa 647 (amino acids 837–853). The Y274fsX variant had no cell-surface HA signal (see Fig 4D). However, in a subsequent experiment, permeabilization prior to anti-HA incubation revealed abundant total expression, suggesting a trafficking defect for Y274fsX36. Y533X exhibited cell-surface HA immunoreactivity (see Fig 4D), indicating that truncated Y533X proteins reach the plasma membrane.

Voltage Dependence of Channel Activation and Inactivation

Voltage dependence of channel activation and inactivation was assessed for K_V2.1 variants with sufficient K^+ conductance to reliably measure these parameters. In the homomeric configuration, several variants exhibited altered voltage dependence of channel activation and inactivation when compared to WT (Table). S202F and R312H exhibited depolarizing shifts in their $V_{1/2}$ for both channel activation and inactivation (see Fig 5A) and larger slope factors, suggesting a decrease in voltage sensitivity for channel inactivation. Y533X induced a depolarizing shift in $V_{1/2}$ of activation without affecting channel inactivation (see Table). In contrast, R325W caused hyperpolarizing shifts in the $V_{1/2}$ values for both channel activation and inactivation (see Fig 5A).

When coexpressed with WT, the effects of R312H on channel activation and inactivation were abolished, suggesting rescue by WT subunits. Coexpression with WT channels prevented the depolarizing shift in activation due to S202F, but did not alter the effects on inactivation (see Fig 5B, Table). Hyperpolarizing shifts in $V_{1/2}$ for activation and inactivation caused by R325W were still evident in the presence of WT, albeit with smaller magnitude. Although T210K was nonfunctional as a homotetramer, it caused a hyperpolarizing shift in inactivation $V_{1/2}$ when coexpressed with WT. A complete summary is presented in the Table.

Functional Effects of Nonpathogenic Variants

Two likely nonpathogenic variants (R325Q, S457R) were included in functional assays, with experimenters blinded to this status. R325Q was present as a singleton variant (minor allele frequency [MAF] = $3.983^{e\text{-}06}$) in the genome aggregation database (gnomAD), which is devoid of individuals with severe pediatric disease.[27] R325Q was indistinguishable from WT in contrast to the disease-associated R325W variant, which induced changes in both channel activation and inactivation (see Fig 5).

S457R was classified as nonpathogenic based on inheritance from an unaffected parent and presence of S457R as a singleton variant (MAF = $3.983^{e\text{-}06}$) in gnomAD.[27] In the homomeric configuration, S457R was indistinguishable from

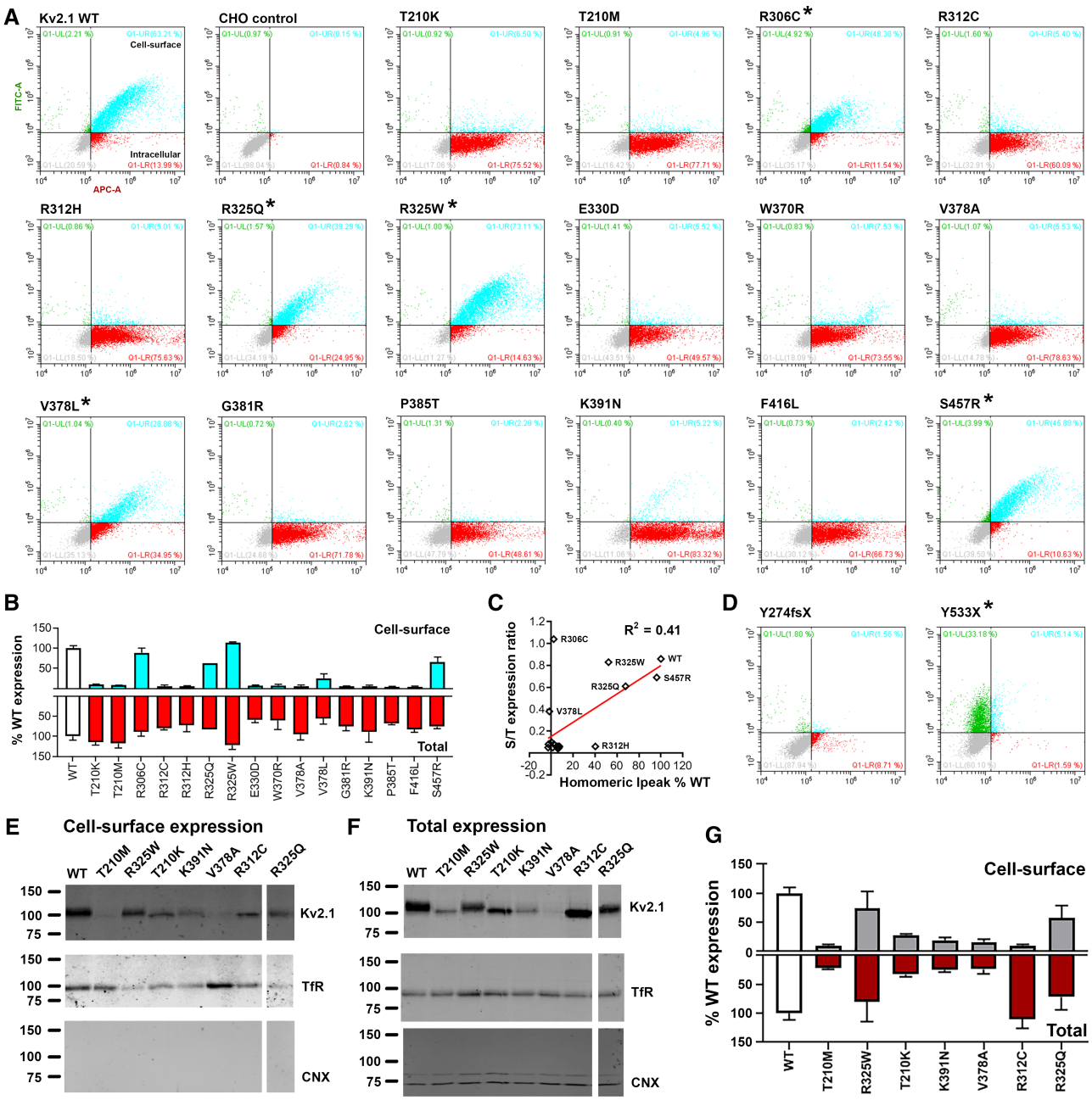

FIGURE 4: Total and cell-surface protein expression levels of $K_V2.1$ variants. (A) Representative dot-plots of flow cytometry analyses of CHO cells expressing $K_V2.1$ tagged with hemagglutinin (HA)-epitope at the extracellular site between S1–S2 linker regions; anti–HA-Alexa 488 and anti–$K_V2.1$-Alexa 647 antibodies were used to probe the cell-surface and intracellular $K_V2.1$, respectively. Population in turquoise ($HA^+/K_V2.1^+$) denotes $K_V2.1$ located at the cell surface, whereas the dots in red ($HA^+/K_V2.1^-$) indicate expressed $K_V2.1$ protein located intracellularly. Wild-type (WT) and nontransfected CHO cells (negative control) are shown at the top left for comparison. Nontransfected CHO cells underwent the entire immunocytochemistry labeling protocol. Asterisks denote variants with intact cell-surface trafficking, ie, S/T ratio > 0.3. (B) Expression level comparisons of $K_V2.1$ variants to that of WT *(white bars)* revealed reduced cell-surface trafficking of variants. Cell-surface expression is shown in turquoise and the total expression in red. (C) Correlational analyses of surface-to-total expression level ratio and homomeric peak current (I_{peak}) density (values in % WT) result in $R^2 = 0.41$ and $p = 0.006$ by Pearson correlation. (D) Analyses of 2 truncation variants, devoid of the epitope site for anti–$K_V2.1$-Alexa 647, further validate the assay. The Y274fsX36 variant fails to reach the cell surface. In contrast, for Y533X, the population in green ($HA^+/K_V2.1^-$) denotes $K_V2.1$ expressed and reaching the cell surface, yet unable to be detected by the anti–$K_V2.1$-Alexa 647 antibody due to the absent epitope. (E, F) Cross-validation analyses of select $K_V2.1$ variants for cell-surface and total protein expression. CNX = calnexin; TfR = transferrin receptor; S/T = surface/total ratio; LL = lower left; LR = lower right; UL = upper left; UR = upper right. (G) Quantification of Western blot analyses confirms similar expression pattern as immunocytochemistry–flow cytometry assay.

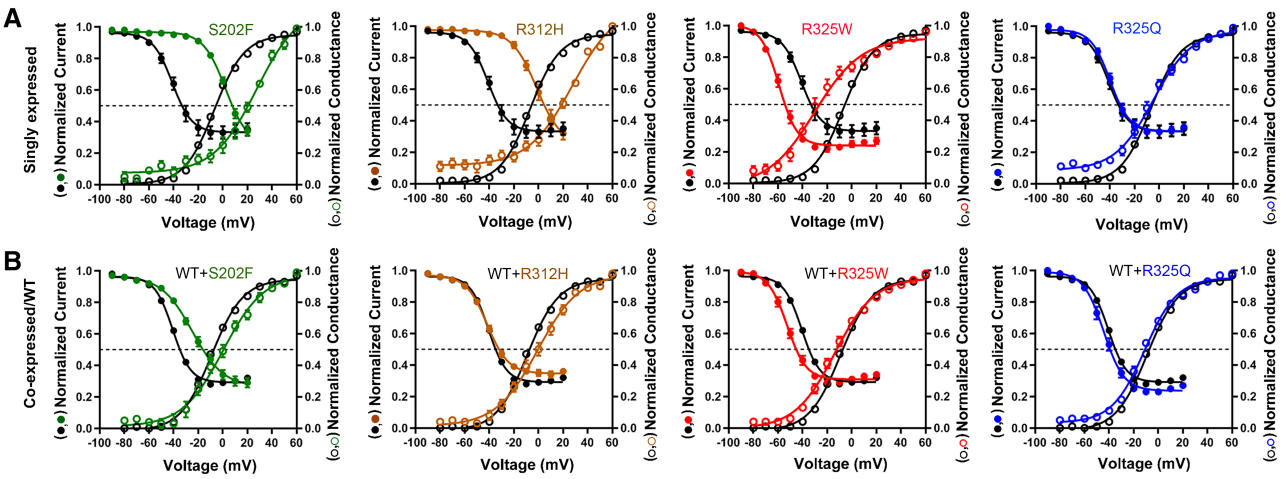

FIGURE 5: Voltage dependence of activation/inactivation of K_V2.1 variants. Voltage-dependent channel activation *(open circles)* and inactivation *(solid circles)* curves obtained from selected homomeric and coexpression K_V2.1 variants are compared to wild type (WT; *black circles*). Solid lines represent averaged data fits with the Boltzmann equation. Numerical values of voltage for half-maximal channel activation and slope factor for the other variants are listed in the Table.

WT. However, there was a hyperpolarizing shift in voltage dependence of activation when S457R was coexpressed with WT. S457 is subject to post-translational phosphorylation, and dephosphorylation of K_V2.1 is associated with hyperpolarizing shifts in voltage-dependent gating.[28] The observed difference in voltage dependence of activation may reflect differences in phosphorylation state between the variant (nonphosphorylated residue 457) and WT subunits (phosphorylated residue 457) under our experimental conditions, which require intracellular sodium fluoride, a phosphatase inhibitor, for gigaohm seal formation.

Genotype–Phenotype Analyses of K_V2.1 Variants

To visualize the relationship among various parameters, we performed PCA using 6 variables measured in the homomeric configuration: I_{peak} density, $V_{1/2}$ and k for activation and inactivation, and cell-surface/total expression ratio (Fig 6). The top 3 leading dimensions for PC1 were I_{peak} density (0.61), cell-surface/total expression ratio (0.62), and $V_{1/2}$ for activation (−0.28); for PC2, they were I_{peak} density (0.62), and inactivation $V_{1/2}$ (0.47) and k (0.49). Plotting PC1 versus PC2 separated nonpathogenic (R325Q, S457R, WT) from pathogenic variants with 95% confidence. However, it was not possible to separate the pathogenic variants by clinical classification.

In addition, we performed correlational analyses with quantifiable clinical phenotypes and the leading variables identified by PCA: conductance and cell-surface/total expression ratio (see Fig 6B–E). Among these parameters, we identified a single correlation between the number of seizure types and conductance (R^2 = 0.19; p < 0.02, Spearman), with low/no conductance associated with a more complex clinical presentation that included multiple seizure types. Conversely, variants with some level of preserved conductance (>0.2 of WT) had only 1 to 2 seizure types, indicative of a less complex clinical presentation.

Discussion

K_V2.1 Loss of Function in KCNB1 *DEE*

Here we report functional studies of 19 *KCNB1* variants, including 17 likely pathogenic variants identified in individuals with DEE or other NDDs, and 2 presumed nonpathogenic variants present in the gnomAD database, which excludes severe pediatric disease.[27] High-throughput electrophysiological and biochemical analysis of K_V2.1 variants expressed in CHO-K1 cells revealed partial or near-complete loss of function as a common mechanism, consistent with prior manual electrophysiology.[7–9] The molecular mechanisms underlying loss-of-function phenotypes included lower I_{peak} density due to low total and/or cell-surface K_V2.1 expression, and shifts in voltage dependence of activation and inactivation.

The majority of variants exhibited significantly lower I_{peak} density when expressed as homotetramers. However, coexpression with WT subunits normalized I_{peak} density for many variants. Rescue by WT subunits suggests that variant subunits traffic to the cell surface as part of a heteromeric assembly, raising the possibility of rescue by molecular chaperones. In contrast, coexpression of some variants (R306C, V378L) with WT resulted in lower I_{peak} density, approximating 0.5× WT, suggesting that although the mutant subunits cannot be rescued, they do not interfere with cell-surface expression of WT. Coexpression of other variants (W370R, P385T, F416L) with WT resulted in I_{peak} density < 0.5× WT, suggesting a dominant-negative effect on cell-surface expression of WT subunits.

TABLE. Biophysical Properties of $K_V2.1$ Variants Singly or Coexpressed with WT

Configurations or Variants	Voltage Dependence of Activation		Voltage Dependence of Inactivation	
	$V_{½}$	*k*	$V_{½}$	*k*
WT	−4.6 ± 1.0	13.0 ± 0.4	−35.5 ± 2.6	7.5 ± 0.6
S202F	24.3 ± 3.8, $p < 0.001$ (n = 14)[a]	16.4 ± 1.7, $p > 0.189$ (n = 14)	2.7 ± 1.2, $p < 0.001$ (n = 30)[a]	8.8 ± 0.4, $p < 0.001$ (n = 30)[a]
R312H	28.1 ± 1.5, $p < 0.001$ (n = 21)[a]	18.2 ± 1.0, $p < 0.001$ (n = 21)[a]	−0.1 ± 2.3, $p < 0.001$ (n = 18)[a]	8.5 ± 0.7, $p < 0.001$ (n = 18)[a]
R325Q	−5.0 ± 2.5, $p > 0.884$ (n = 18)	14.8 ± 1.2, $p > 0.804$ (n = 18)	−39.6 ± 1.8, $p > 0.704$ (n = 17)	7.1 ± 0.4, $p > 0.083$ (n = 17)
R325W	−23.4 ± 3.9, $p < 0.001$ (n = 22)[a]	17.7 ± 1.2, $p > 0.033$ (n = 22)	−58.0 ± 1.4, $p < 0.001$ (n = 25)[a]	5.7 ± 0.2, $p < 0.001$ (n = 25)[a]
S457R	−13.3 ± 1.4, $p > 0.050$ (n = 25)	12.0 ± 0.7, $p > 0.952$ (n = 25)	−44.2 ± 1.7, $p > 0.543$ (n = 38)	6.5 ± 0.2, $p > 0.418$ (n = 38)
Y533X	13.0 ± 3.6, $p < 0.001$ (n = 17)[a]	18.3 ± 1.4, $p < 0.001$ (n = 17)[a]	−45.7 ± 2.6, $p > 0.313$ (n = 26)	6.8 ± 0.6, $p > 0.200$ (n = 26)
WT + WT	−7.3 ± 0.9	12.9 ± 0.9	−39.6 ± 0.6	6.3 ± 0.1
WT + S202F	1.3 ± 3.1, $p > 0.184$ (n = 25)	22.2 ± 0.8, $p < 0.001$ (n = 25)[a]	−29.6 ± 1.7, $p < 0.001$ (n = 54)[a]	10.4 ± 0.4, $p < 0.001$ (n = 54)[a]
WT + T210K	−10.8 ± 1.3, $p > 0.395$ (n = 44)	13.1 ± 0.5, $p > 0.999$ (n = 44)	−46.2 ± 1.3, $p < 0.001$ (n = 34)[a]	6.3 ± 0.2, $p > 0.999$ (n = 34)
WT + T210M	−6.9 ± 1.7, $p > 0.999$ (n = 29)	12.9 ± 0.9, $p > 0.999$ (n = 29)	−43.3 ± 2.4, $p > 0.917$ (n = 25)	6.5 ± 0.3, $p > 0.996$ (n = 25)
WT + Y274fsX	−7.1 ± 4.0, $p > 0.999$ (n = 18)	14.5 ± 1.1, $p > 0.949$ (n = 18)	−40.2 ± 1.6, $p > 0.999$ (n = 65)	5.7 ± 0.2, $p > 0.380$ (n = 65)
WT + R306C	−15.9 ± 3.7, $p > 0.435$ (n = 11)	15.3 ± 2.2, $p > 0.989$ (n = 11)	−44.9 ± 3.2, $p > 0.847$ (n = 22)	9.0 ± 0.6, $p < 0.003$ (n = 22)[a]
WT + R312C	−9.1 ± 1.3, $p > 0.989$ (n = 35)	13.4 ± 0.5, $p > 0.999$ (n = 35)	−42.0 ± 1.3, $p > 0.850$ (n = 27)	6.0 ± 0.1, $p > 0.946$ (n = 27)
WT + R312H	0.1 ± 2.7, $p > 0.198$ (n = 31)	14.3 ± 0.7, $p > 0.776$ (n = 31)	−38.7 ± 1.5, $p > 0.999$ (n = 78)	7.7 ± 0.4, $p > 0.010$ (n = 78)
WT + R325Q	−10.7 ± 1.4, $p > 0.527$ (n = 43)	12.8 ± 0.6, $p > 0.999$ (n = 43)	−43.4 ± 1.7, $p > 0.531$ (n = 32)	5.9 ± 0.2, $p > 0.957$ (n = 32)
WT + R325W	−14.3 ± 1.7, $p < 0.011$ (n = 39)[a]	16.1 ± 1.0, $p > 0.077$ (n = 39)	−51.9 ± 1.5, $p < 0.001$ (n = 35)[a]	5.9 ± 0.2, $p > 0.957$ (n = 35)
WT + E330D	−12.4 ± 2.3, $p > 0.529$ (n = 18)	15.3 ± 1.4, $p > 0.825$ (n = 18)	−40.4 ± 2.3, $p > 0.999$ (n = 52)	7.4 ± 1.0, $p > 0.987$ (n = 52)
WT + W370R	−3.5 ± 3.3, $p > 0.986$ (n = 12)	16.4 ± 1.8, $p > 0.663$ (n = 12)	−38.9 ± 2.9, $p > 0.999$ (n = 26)	6.9 ± 0.4, $p > 0.813$ (n = 26)
WT + V378A	−7.5 ± 1.4, $p > 0.999$ (n = 29)	13.3 ± 0.5, $p > 0.999$ (n = 29)	−41.4 ± 1.2, $p > 0.976$ (n = 32)	5.6 ± 0.2, $p > 0.159$ (n = 32)
WT + V378L	−5.8 ± 4.8, $p > 0.999$ (n = 20)	16.0 ± 1.2, $p > 0.298$ (n = 20)	−46.4 ± 1.9, $p > 0.022$ (n = 61)	7.5 ± 0.3, $p < 0.003$ (n = 61)
WT + G381R	−9.4 ± 2.7, $p > 0.999$ (n = 27)	14.2 ± 1.0, $p > 0.916$ (n = 27)	−41.2 ± 1.4, $p > 0.995$ (n = 62)	6.3 ± 0.5, $p > 0.999$ (n = 62)
WT + P385T	−6.7 ± 4.1, $p > 0.999$ (n = 11)	14.9 ± 1.2, $p > 0.850$ (n = 11)	−40.6 ± 2.1, $p > 0.999$ (n = 43)	6.9 ± 0.5, $p > 0.958$ (n = 43)
WT + K391N	−9.4 ± 1.2, $p > 0.947$ (n = 44)	12.6 ± 0.4, $p > 0.999$ (n = 44)	−41.4 ± 1.2, $p > 0.977$ (n = 39)	5.9 ± 0.1, $p > 0.492$ (n = 39)
WT + F416L	−3.1 ± 3.7, $p > 0.988$ (n = 16)	15.6 ± 1.1, $p > 0.388$ (n = 16)	−39.5 ± 1.6, $p > 0.999$ (n = 48)	7.3 ± 0.4, $p > 0.175$ (n = 48)
WT + S457R	−18.9 ± 3.0, $p < 0.019$ (n = 22)[a]	14.1 ± 1.0, $p > 0.989$ (n = 22)	−42.0 ± 1.6, $p > 0.960$ (n = 42)	5.9 ± 0.2, $p > 0.959$ (n = 42)
WT + Y533X	−11.6 ± 1.7, $p > 0.384$ (n = 42)	14.8 ± 0.8, $p > 0.468$ (n = 42)	−43.0 ± 1.4, $p > 0.432$ (n = 65)	6.0 ± 0.2, $p > 0.998$ (n = 65)

Singly expressed variants with at least 10pA/pF are included; n = the number of cells recorded.
[a]Values that differ from the respective WT condition (Dunnett T3 multiple comparisons).
k = slope factor; $V_{½}$ = voltage for half-maximal channel activation; WT = wild type.

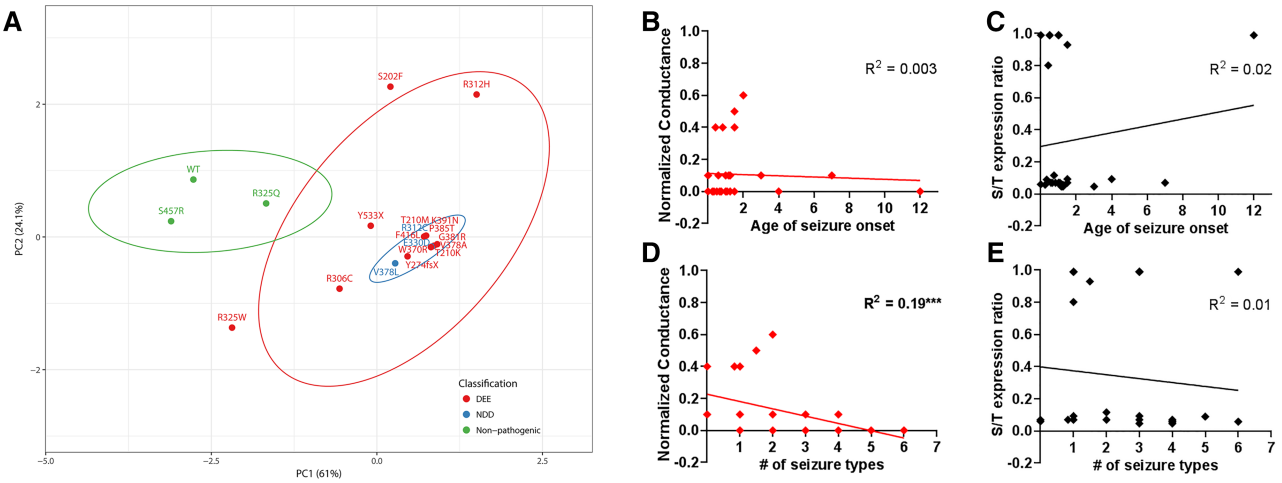

FIGURE 6: Principal component analyses of K_V2.1 variants. (A) Experimental data for biophysical and protein expression analyses were transformed with respect to wild type (WT), to generate eigenvector-based multivariate analyses, and plotted using ClustVis.[20] Nipals principal component analysis is used to calculate principal components, with ellipses depicting 95% confidence interval. Each axis explains 61% and 24.1% of the total variance (x and y, respectively); n = 20 data points. Six variables measured in the homomeric condition were used: peak current (I_{peak}) density, voltage for half-maximal channel activation ($V_{½}$) and slope factor (*k*) for activation and inactivation, and protein expression cell-surface/total ratio. The top 3 leading dimensions (variable) for principal component 1 (PC1) were I_{peak} density (0.61), cell-surface/total expression ratio (0.62), and $V_{1/2}$ for activation (−0.28); for PC2, they were I_{peak} density (0.62), inactivation $V_{1/2}$ (0.47), and *k* (0.49). Nonpathogenic variants and WT (in green) are separable from the pathogenic variants (red, blue). DEE = developmental epileptic encephalopathy; NDD = neurodevelopmental disorder. (B–E) Correlational analysis of quantifiable clinical parameters and the leading functional parameters identified in this study. Conductance values normalized to that of WT and surface-to-total protein expression ratio were used for analyses. R^2 values are noted for each plot (*$p < 0.02$, Spearman).**

Several variants encoded functional K_V2.1 channels with I_{peak} density indistinguishable from WT, but with defects in voltage dependence. Depolarizing shifts in $V_{1/2}$ for both activation and inactivation were observed for S202F and R312H, resulting in loss of function due to impaired channel opening in a physiological voltage range. Conversely, R325W had hyperpolarized shifts in $V_{1/2}$ for activation and inactivation. Although this likely results in enhanced channel opening at physiological voltages, the corresponding shift in the voltage dependence of inactivation limits channel availability, suggesting overall loss of function. Coexpression of WT channels to approximate heterozygosity resulted in attenuated or altered voltage dependence. This may be explained by variable populations of WT + WT, WT + variant, and variant+variant channels. The presence of significant voltage dependence phenotypes specific to coexpression conditions (activation *k* for WT + S202F or activation $V_{1/2}$ for WT + S457R) suggests that some variants coassemble with WT subunits as heterotetramers.

Comparison of Same-Site Substitutions

The importance of experimental validation is highlighted by pairwise comparison of substitutions of different amino acids at the same position (T210K/M, R312C/H, R325Q/W, and V378A/L). The T210K/M variants resulted in loss of K^+ conductance and cell-surface K_V2.1 expression. T210 is a critical residue forming the S1–pore interface.[31,32] A hydroxyl group is required at this position for channel function.[32] Thus, substitution with either lysine or methionine would be incompatible with channel function. In contrast, R312H and R312C resulted in partial and severe loss of conductance, respectively, which was opposite of the in silico consequence prediction that suggested R312H would be more deleterious than R312C (see Supplementary Table 1). Retaining a positive charge at this position in the S4 segment by substituting histidine may lessen severity relative to a charge-neutralization cysteine substitution. Similarly, the R325Q/W variants differed in their voltage dependence, with R325Q retaining WT-like behavior, consistent with nonpathogenicity. This suggests that substitution of R325 with a bulky hydrophobic tryptophan may alter electrochemical coupling between S4–S5 and the S6 segment,[33] whereas glutamine is tolerated.

Both the V378A/L variants resulted in loss of K^+ conductance in the absence of WT subunits. V378L exhibited modest cell-surface expression, whereas the V378A variant was absent, suggesting discrete mechanisms underlying loss of K^+ conductance for these variants. Leucine is present at the equivalent position in K_V3 and K_V4 channels, indicating that this substitution is structurally tolerable and maintains K^+ selectivity, although it likely alters conductance.[34,35] Conversely, substitution with alanine has been shown to disrupt ion selectivity and affect channel stability.[35] Previous studies of the V378A variant in CHO-K1 and COS-7 cells showed

impaired expression that could be rescued by the K_V2 inhibitor GxTx, suggesting enhanced internalization and degradation as a possible mechanism.[9] Consistent with this, we observed robust total expression of V378A at 24 hours post-transfection (see Fig 4), whereas there was little V378A expression at 72 hours (see Fig 4E–G).

High-Throughput Variant Characterization Pipeline

One goal of this study was to optimize electroporation and automated planar patch clamp technologies for high-throughput characterization of *KCNB1* variants identified by clinical genetic testing, making it feasible to rapidly characterize new variants. Moreover, the ICC-FC assay enables high-throughput evaluation of cell-surface and total protein expression for further delineation of pathogenic mechanisms. Efficient functional characterization of ion channel variants is critical to realize the precision medicine goal of rapid, definitive precision diagnosis and targeted treatment based on the specific genetic variant.

Utility of Functional Characterization for Clinical Genetic Testing

Based on American College of Medical Genetics and Genomics guidelines, evidence of a deleterious effect on protein function can be considered "strong" evidence for pathogenicity, given the functional assay is robust and validated.[3] Electrophysiology is the gold standard for characterizing the effects of ion channel variants, and is a well-validated, robust approach. In contrast, in silico evidence based on pathogenicity prediction algorithms are only considered "supporting" evidence, insufficient when considered alone. Functional variant characterization, both in channelopathies and in other disorders, has untapped potential to provide diagnostic benefit for weighing variant pathogenicity. Functional characterization of a series of *KCNB1* variants can serve as a reference dataset for genetic test interpretation in newly diagnosed patients, and provide additional evidence for reclassification of variants previously classified as variants of uncertain significance.

The *KCNB1* variants R325Q and S457R provide examples of how functional variant characterization can provide useful information. R325Q is a rare population variant that exhibited similar functional characteristics to WT channels, demonstrating that glutamine substitution at R325 is tolerated. However, R325W had significant functional defects as a homotetramer and when coexpressed with WT (see Fig 2C, D), supporting this variant as potentially pathogenic. S457R was initially identified by clinical genetic testing in a child with DEE, but was later found to be inherited from an unaffected parent. Prior to parental testing, we performed electrophysiological characterization of S457R and found no deleterious effect on protein function, consistent with nonpathogenicity. PCA allowed reliable separation of the nonpathogenic group (R325Q, S457R, WT) from the other 17 variants studied, highlighting the viability of functional screening to differentiate nonpathogenic versus pathogenic variants with high confidence (95%).

Genotype–Phenotype Correlations

Another goal of our study was to assess potential correlations between $K_V2.1$ channel dysfunction and clinical severity. Although the clinical phenotypes of DEE and other NDDs were not distinguished by PCA, it is possible that the NDD cases (3–6 years of age at the time of reporting) will go on to develop epilepsy, as there are at least 2 DEE cases with seizure onset in adolescence (see Supplementary Table 1). We identified a correlation between conductance and the number of seizure types, indicating that variants with preserved functionality are associated with less complex epilepsy. However, due to the higher likelihood of genetic testing in complex epilepsy cases, our cohort is biased toward the more severe end of the spectrum. Characterization of additional variants across a broad clinical spectrum may help establish clearer genotype–phenotype correlations. Alternatively, the underlying pathogenic mechanisms may require more complex experimental systems, and/or final expression of the clinical phenotype can be influenced by other genetic, epigenetic, or environmental modifiers. The variable severity observed among patients with the same recurrent variant is consistent with other factors contributing to clinical presentation.

Limitations of High-Throughput Functional Screening

Despite the aforementioned strengths of functional evaluation in a heterologous expression model, there are some limitations. Some $K_V2.1$ variant effects detected in our study may become more or less pronounced in neurons. For example, variant and WT alleles are coexpressed in individuals with *KCNB1* DEE, which is associated with heterozygous variants. However, in CHO-K1 cells, coexpression with WT sometimes masked variant effects. This highlights a difference between heterologous expression versus the nervous system and suggests that homomeric expression provides a more robust assay. In neurons, a population of nonconducting $K_V2.1$ clustered at plasma membrane–endoplasmic reticulum junctions operates as a docking site for membrane proteins,[30] a function that is not assessed in our system. In addition, the effect of variants that alter binding site affinity for interacting proteins like KChAP, AMIGO, and KCNE1-3[36–38] may not be detected if interacting proteins are not present at relevant levels in CHO-K1 cells. Hence, additional characterization of variants in more complex experimental systems will be necessary for complete

understanding of disease mechanisms in neurons and other specialized cells where K_V2.1 is a significant contributor.

Conclusions

Efficient characterization of *KCNB1* variants can provide the precision diagnoses required for precision medicine. Many of the disease-associated *KCNB1* variants (14/17) exhibited phenotypes that ultimately result in a channel hypofunction, through (1) decreased K^+ conductance, (2) altered voltage dependence, (3) reduced protein expression, or (4) altered cell-surface trafficking. Classification of *KCNB1* variants into categories of defects suggests that molecular chaperones to increase cell-surface expression may be a suitable therapeutic strategy for some, whereas subtype-selective activators of K_V2.1 may be a viable therapy for others. Alternatively, antisense oligonucleotide or gene therapy approaches that increase expression may hold promise for treatment of *KCNB1* DEE.

Note in proof: An additional clinical paper describing KCNB1 DEE was recently published. Bar, C, Barcia, G, Jennesson, M, et al. Expanding the genetic and phenotypic relevance of KCNB1 variants in developmental and epileptic encephalopathies: 27 new patients and overview of the literature. Human Mutation. 2019; 1–12. https://doi.org/10.1002/humu.23915.

Acknowledgment

This work was supported by funding from NIH National Institute of Neurological Disorders and Stroke grants R01 NS053792 (J.A.K.), U54 NS108874 (A.L.G.), and K08 NS097633 (E.M.G.), the Ann & Robert H. Lurie Children's Hospital of Chicago Precision Medicine Initiative (J.J.M., J.B.O., S.N.M.), and the Pediatric Physician-Scientist Research Award (S.N.M.). A.T. is supported by Scripps Research Translational Institute and an NIH National Center for Advancing Translation Sciences Clinical and Translational Science Award (5 UL1 TR001114). A.P. was supported by the Translational Research Program, Boston Children's Hospital. S.K.K. is supported by a predoctoral fellowship from the American Epilepsy Society.

We thank the patients and their families for their cooperation; and T. Abramova, R. Desai, N. Hawkins, T. Thaxton, and A. Huffman for technical assistance.

Author Contributions

C.G.V., A.L.G., and J.A.K. contributed to the conception and design of the study. S.K.K., C.G.V., D.M.E., J.D.C., S.N.M., J.B.O., K.L.F., D.M., L.D., P.G., L.E.G., I.T., C.S., K.A.S., A.T., J.v.d.S., K.v.G., R.P.C., J.D., E.L., J.E.J., M.C.H., J.L., N.R.F., A.S., B.L., A.P., E.D.M., E.M.G., J.J.M., and J.A.K. contributed to acquisition and analysis of the data. S.K.K., C.G.V., S.N.M., A.L.G., and J.A.K. contributed to drafting the text and preparing figures.

Potential Conflicts of Interest

D.M. is employed by GeneDx, a wholly owned subsidiary of OPKO Health, which provides genetic testing that includes *KCNB1* on epilepsy and autism spectrum disorders/intellectual disability panels. The other authors report no competing interests related to this study.

References

1. Allen AS, Berkovic SF, Cossette P, et al. De novo mutations in epileptic encephalopathies. Nature 2013;501:217–221.
2. Carvill GL, Mefford HC. Next-generation sequencing in intellectual disability. J Pediatr Genet 2015;4:128–135.
3. Richards S, Aziz N, Bale S, et al. Standards and guidelines for the interpretation of sequence variants: a joint consensus recommendation of the American College of Medical Genetics and Genomics and the Association for Molecular Pathology. Genet Med 2015;17:405–424.
4. Murakoshi H, Trimmer JS. Identification of the Kv2.1 K+ channel as a major component of the delayed rectifier K+ current in rat hippocampal neurons. J Neurosci 1999;19:1728–1735.
5. Bishop HI, Guan D, Bocksteins E, et al. Distinct cell- and layer-specific expression patterns and independent regulation of Kv2 channel subtypes in cortical pyramidal neurons. J Neurosci 2015;35:14922–14942.
6. Speca DJ, Ogata G, Mandikian D, et al. Deletion of the Kv2.1 delayed rectifier potassium channel leads to neuronal and behavioral hyperexcitability. Genes Brain Behav 2014;13:394–408.
7. Torkamani A, Bersell K, Jorge BS, et al. De novo KCNB1 mutations in epileptic encephalopathy. Ann Neurol 2014;76:529–540.
8. Saitsu H, Akita T, Tohyama J, et al. De novo KCNB1 mutations in infantile epilepsy inhibit repetitive neuronal firing. Sci Rep 2015;5:15199.
9. Thiffault I, Speca DJ, Austin DC, et al. A novel epileptic encephalopathy mutation in KCNB1 disrupts Kv2.1 ion selectivity, expression, and localization. J Gen Physiol 2015;146:399–410.
10. Latypova X, Matsumoto N, Vinceslas-Muller C, et al. Novel KCNB1 mutation associated with non-syndromic intellectual disability. J Hum Genet 2017;62:569–573.
11. de Kovel CGF, Syrbe S, Brilstra EH, et al. Neurodevelopmental disorders caused by de novo variants in KCNB1 genotypes and phenotypes. JAMA Neurol 2017;74:1228–1236.
12. Allen NM, Conroy J, Shahwan A, et al. Unexplained early onset epileptic encephalopathy: exome screening and phenotype expansion. Epilepsia 2016;57:e12–e17.
13. Miao P, Peng J, Chen C, et al. A novel mutation in KCNB1 gene in a child with neuropsychiatric comorbidities with both intellectual disability and epilepsy and review of literature [in Chinese]. Zhonghua Er Ke Za Zhi 2017;55:115–119.
14. Calhoun JD, Vanoye CG, Kok F, et al. Characterization of a KCNB1 variant associated with autism, intellectual disability, and epilepsy. Neurol Genet 2017;3:e198.
15. Fitzgerald TW, Gerety SS, Jones WD, et al. Large-scale discovery of novel genetic causes of developmental disorders. Nature 2015;519:223–228.

16. Marini C, Romoli M, Parrini E, et al. Clinical features and outcome of 6 new patients carrying de novo KCNB1 gene mutations. Neurol Genet 2017;3:e206.

17. Landrum MJ, Lee JM, Benson M, et al. ClinVar: improving access to variant interpretations and supporting evidence. Nucleic Acids Res 2018;46:D1062–D1067.

18. Lek M, Karczewski KJ, Minikel EV, et al. Analysis of protein-coding genetic variation in 60,706 humans. Nature 2016;536:285–291.

19. Swaminathan GJ, Bragin E, Chatzimichali EA, et al. DECIPHER: Web-based, community resource for clinical interpretation of rare variants in developmental disorders. Hum Mol Genet 2012;21:R37–R44.

20. Metsalu T, Vilo J. ClustVis: a Web tool for visualizing clustering of multivariate data using principal component analysis and heatmap. Nucleic Acids Res 2015;43:W566–W570.

21. Long SB, Tao X, Campbell EB, MacKinnon R. Atomic structure of a voltage-dependent K+ channel in a lipid membrane-like environment. Nature 2007;450:376–382.

22. Long SB, Campbell EB, Mackinnon R. Voltage sensor of Kv1.2: structural basis of electromechanical coupling. Science 2005;309: 903–908.

23. Taglialatela M, Drewe JA, Brown AM. Barium blockade of a clonal potassium channel and its regulation by a critical pore residue. Mol Pharmacol 1993;44:180–190.

24. Kircher M, Witten DM, Jain P, et al. A general framework for estimating the relative pathogenicity of human genetic variants. Nat Genet 2014;46:310–315.

25. Vanoye CG, Desai RR, Fabre KL, et al. High-throughput functional evaluation of KCNQ1 decrypts variants of unknown significance. Circ Genom Precis Med 2018;11:e002345.

26. Huang H, Kuenze G, Smith JA, et al. Mechanisms of KCNQ1 channel dysfunction in long QT syndrome involving voltage sensor domain mutations. Sci Adv 2018;4:eaar2631.

27. Karczewski KJ, Francioli LC, Tiao G, et al. Variation across 141,456 human exomes and genomes reveals the spectrum of loss-of-function intolerance across human protein-coding genes. bioRxiv 2019:531210.

28. Cerda O, Baek JH, Trimmer JS. Mining recent brain proteomic databases for ion channel phosphosite nuggets. J Gen Physiol 2011; 137:3–16.

29. Fox PD, Loftus RJ, Tamkun MM. Regulation of Kv2.1 K(+) conductance by cell surface channel density. J Neurosci 2013;33: 1259–1270.

30. Deutsch E, Weigel AV, Akin EJ, et al. Kv2.1 cell surface clusters are insertion platforms for ion channel delivery to the plasma membrane. Mol Biol Cell 2012;23:2917–2929.

31. Full Y, Seebohm G, Lerche H, Maljevic S. A conserved threonine in the S1-S2 loop of KV7.2 and K V7.3 channels regulates voltage-dependent activation. Pflugers Archiv 2013;465:797–804.

32. Lee SY, Banerjee A, MacKinnon R. Two separate interfaces between the voltage sensor and pore are required for the function of voltage-dependent K(+) channels. PLoS Biol 2009;7:e47.

33. Betts MJ Russell RB. Amino acid properties and consequences of substitutions. In: Gray IC, Barnes MR, eds. *Bioinformatics for geneticists*. Hoboken, NJ: John Wiley & Sons, 2003:289–316.

34. Brown AM, Drewe JA, Hartmann HA, et al. The potassium pore and its regulation. Ann N Y Acad Sci 1993;707:74–80.

35. Heginbotham L, Lu Z, Abramson T, MacKinnon R. Mutations in the K + channel signature sequence. Biophys J 1994;66:1061–1067.

36. Peltola MA, Kuja-Panula J, Lauri SE, et al. AMIGO is an auxiliary subunit of the Kv2.1 potassium channel. EMBO Rep 2011;12: 1293–1299.

37. Kuryshev YA, Gudz TI, Brown AM, Wible BA. KChAP as a chaperone for specific K(+) channels. Am J Physiol Cell Physiol 2000;278: C931–C941.

38. McCrossan ZA, Roepke TK, Lewis A, et al. Regulation of the Kv2.1 potassium channel by MinK and MiRP1. J Membr Biol 2009; 228:1–14.

39. Sievers F, Wilm A, Dineen D, et al. Fast, scalable generation of high-quality protein multiple sequence alignments using Clustal Omega. Mol Syst Biol 2011;7:539.

40. Omasits U, Ahrens CH, Muller S, Wollscheid B. Protter: interactive protein feature visualization and integration with experimental proteomic data. Bioinformatics 2014;30:884–886.